Soft Matter

SUPPLEMENTAL INFORMATION

Understanding the role of crosslink density and linear viscoelasticity on the shear failure of pressure-sensitive-adhesives

Anthony Arrowood,[a] Mohammad A. Ansari,[b] Matteo Ciccotti,[c] Rui Huang,[b] Kenneth M. Liechti,[b] and Gabriel E. Sanoja,[a,*]

[a] *McKetta Department of Chemical Engineering. The University of Texas at Austin, Austin, TX 78712, USA*
[b] *Aerospace Engineering and Engineering Mechanics. The University of Texas at Austin, Austin, TX 78712, USA*
[c] *Laboratoire Sciences et Ingénierie de la Matière Molle. ESPCI Paris, Université PSL, Sorbonne Université, CNRS UMR 7615, 75005 Paris, France*

Contents

List of Figures

1 Limitations of the Study

As noted in the works of Hui *et al.* and Liu *et al.*, the stresses in the adhesive layer are not only shear stresses[1,2]. Their non-linearly elastic model suggests that large normal stresses (parallel and normal to the substrate) are present in the adhesive layer. Here, we restricted our attention to the shear stress in the adhesive layer, assuming that it is homogeneous throughout the adhesive thickness. Future work detailing the triaxial stress distribution in the adhesive layer would refine our understanding of shear failure in PSAs.

We also restricted our attention to the effect of bond length on the shear failure of a family of PSAs. However, it should be noted that the load-bearing area and, more importantly, the shear stress also change. Thus, future work might benefit from decoupling the roles of load and geometry on shear failure.

Finally, we note that the LDPE backing layer slightly creeps, meaning that it is not perfectly elastic. We considered stiffer and thicker backing layers, but these result in much smaller strains in the backing layer and therefore an unacceptably large signal-to-noise ratio in the digital image correlation.

2 Shear Lag Model

2.1 Linearly Visco-elastic Shear Lag Model

Table S1 Table of Symbols.

σ	Axial stress in the backing layer
τ	Shear stress in the adhesive layer
ε	Axial strain in the backing layer
γ	Shear strain in the adhesive layer
h_b	Thickness of the backing layer
h_a	Thickness of the adhesive layer
w	Widith of the tape
δ	Displacement of the backing layer
E	Elastic modulus of the backing layer
G	Shear modulus of the adhesive layer (linearly elastic)
G_0	Shear modulus of the adhesive layer (Kelvin or Maxwell Model)
η	Shear viscosity of the adhesive layer (Kelvin or Maxwell Model)
P	Force applied (normalized to a unit width) [N/m]
L_{LT}	Load transfer length
t_R	Relaxation time

The shear lag model starts with the equilibrium expression relating the shear stress in the adhesive layer of the PSA with the axial stress in the backing layer (see Figure S1) :

$$\tau = h_b \frac{d\sigma}{dx} \tag{S1}$$

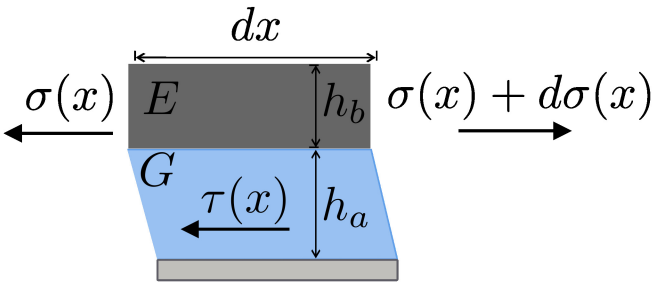

Fig. S1 Geometry of a tape subject to shear loads.

The kinematic equation relating the backing axial displacement to the backing axial strain is the following:

$$\varepsilon = \frac{d\delta}{dx} \tag{S2}$$

and the kinematic equation relating the displacements on the backing layer to the shear strains in the adhesive layer:

$$\gamma = \frac{\delta}{h_a} \tag{S3}$$

The constitutive equation for the backing layer (which is assumed to behave linearly elastic) is the following:

$$\sigma = E\varepsilon \tag{S4}$$

Inserting σ defined by Equation (S4) into (S1), ε defined by Equation (S2), and finally γ defined by (S3), yields the following:

$$\tau = h_b \frac{\partial \sigma}{\partial x} = h_b E \frac{\partial \varepsilon}{\partial x} = h_b E \frac{\partial^2 \delta}{\partial x^2} = h_a h_b E \frac{\partial^2 \gamma}{\partial x^2} \tag{S5}$$

There are two boundary conditions required. First, the stress at the edge of the substrate is that of the applied load

$$\sigma|_{x=0} = -\frac{P}{w h_b} \tag{S6}$$

In terms of shear strain in the adhesive layer, utilizing Equations (S2), (S3) and (S4), the first boundary condition is:

$$\frac{d\gamma}{dx}|_{x=0} = \frac{P}{h_a h_b E w} \tag{S7}$$

and second, the stress at the trailing end of the tape is zero.

$$\sigma|_{x=L} = 0 \tag{S8}$$

In terms of shear strain, this boundary condition is:

$$\frac{d\gamma}{dx}|_{x=L} = 0 \tag{S9}$$

For a linearly elastic adhesive, the constitutive equation for the adhesive is given by:

$$\tau = G\gamma \tag{S10}$$

Inserting Equation (S10) into Equation (S5) yields:

$$\tau = \frac{h_a h_b E}{G} \frac{d^2 \tau}{dx^2} \tag{S11}$$

Which may be expressed as

$$\frac{d^2\tau}{d\bar{x}^2} = \tau \tag{S12}$$

where $\bar{x} \equiv x/L_{LT}$ with $L_{LT} \equiv \sqrt{\frac{h_a h_b E}{G}}$ defined as the *Load Transfer Length*. The general solution to this ordinary differential equation is the following:

$$\tau(\bar{x}) = c_1 e^{\bar{x}} + c_2 e^{-\bar{x}} \tag{S13}$$

Converting the first boundary condition to a condition on shear stress:

$$\frac{d\gamma}{dx}|_{x=0} = -\frac{P}{h_a h_b E w} \tag{S14}$$

$$\frac{d\tau}{dx}|_{x=0} = -\frac{PG}{h_a h_b E w} \tag{S15}$$

$$\frac{d\tau}{dx}|_{x=0} = \frac{-P}{L_{LT}^2 w} \tag{S16}$$

$$\frac{d\tau}{d\bar{x}}|_{\bar{x}=0} = \frac{-P}{L_{LT} w} \tag{S17}$$

Applying the first boundary condition:

$$\frac{d\tau}{d\bar{x}}|_{\bar{x}=0} = \frac{-P}{L_{LT} w} = c_1 - c_2$$

and applying the second boundary condition:

$$\frac{d\tau}{d\bar{x}}|_{\bar{x}=\bar{L}} = 0 \tag{S18}$$

$$0 = c_1 e^{\bar{L}} - c_2 e^{-\bar{L}} \ \rightarrow c_2 = c_1 e^{2\bar{L}} \tag{S19}$$

$$c_1 = \frac{-P}{L_{LT} w \left(1 - e^{2\bar{L}}\right)} \tag{S20}$$

$$c_2 = \frac{-P e^{2\bar{L}}}{L_{LT} w \left(1 - e^{2\bar{L}}\right)} \tag{S21}$$

$$\tau(\bar{x}) = \frac{-P}{L_{LT}w}\frac{\left(e^{-\bar{x}} + e^{2\bar{L}\bar{x}}\right)}{\left(1 - e^{2\bar{L}}\right)} \tag{S22}$$

$$= \frac{P}{L_{LT}w}\frac{\left(e^{\left(\bar{L}-\bar{x}\right)} + e^{-(\bar{L}-\bar{x})}\right)}{\left(e^{\bar{L}} - e^{-\bar{L}}\right)} \tag{S23}$$

$$\tau(x) = \frac{P}{L_{LT}w}\frac{\cosh(\bar{L}-\bar{x})}{\sinh(\bar{L})} \tag{S24}$$

The Kelvin solid constitutive expression is the following:

$$\tau = G_0\gamma + \eta\frac{\partial\gamma}{\partial t} \tag{S25}$$

Combining Equations (S25) and (S5) yields:

$$h_a h_b E\frac{\partial^2\gamma}{\partial x^2} = G_0\gamma + \eta\frac{\partial\gamma}{\partial t} \tag{S26}$$

$$\frac{\partial^2\gamma}{\partial x^2} = \frac{G_0}{h_a h_b E}\left(\gamma + \frac{\eta}{G_0}\frac{\partial\gamma}{\partial t}\right) \tag{S27}$$

Equation (S27) does not have a simple solution. The transform to the Laplace domain, imposing the initial condition $\gamma(\bar{x},\bar{t}=0)=0$, yields:

$$\frac{\partial^2 U}{\partial x^2} = U\left(\left(s\frac{\eta}{G_0}+1\right)\frac{G_0}{h_a h_b E}\right) \tag{S28}$$

If an effective load transfer length ($L^*_{LT(s)}$) is defined for the Kelvin solid as:

$$L^*_{LT(s)} \equiv \left(\left(s\frac{\eta}{G_0}+1\right)\frac{G_0}{h_a h_b E}\right)^{-1/2} \tag{S29}$$

then (S28) may be expressed in the form of Equation (S12):

$$\frac{\partial^2 U}{\partial \bar{x}^2} = U \tag{S30}$$

with $\bar{x} = x/L^*_{LT(s)}$ and solved in the similar manner:

$$U(\bar{x}) = c_1 e^{\bar{x}} + c_2 e^{-\bar{x}} \tag{S31}$$

Applying the first boundary condition:

$$\frac{dU}{d\bar{x}}|_{\bar{x}=0} = \left(-\frac{1}{s} \frac{L^*_{LT(s)} P}{h_a h_b E w} \right) \tag{S32}$$

$$c_1 - c_2 = \left(-\frac{1}{s} \frac{L^*_{LT(s)} P}{h_a h_b E w} \right) \tag{S33}$$

and applying the second boundary condition:

$$0 = c_1 e^{\bar{L}} - c_2 e^{-\bar{L}} \ \rightarrow c_2 = c_1 e^{2\bar{L}} \tag{S34}$$

$$c_1 - c_1 e^{2\bar{L}} = \left(\frac{1}{s} \frac{L^*_{LT(s)} P}{h_a h_b E w} \right) \tag{S35}$$

$$c_1 \left(1 - e^{2\bar{L}} \right) = \left(\frac{1}{s} \frac{L^*_{LT(s)} P}{h_a h_b E w} \right) \tag{S36}$$

$$c_1 = \frac{\left(\frac{1}{s} \frac{L^*_{LT(s)} P}{h_a h_b E w} \right)}{\left(1 - e^{2\bar{L}} \right)} \tag{S37}$$

$$\tag{S38}$$

$$U(\bar{x}) = c_1 e^{\bar{x}} + c_1 e^{2\bar{L}} e^{-\bar{x}} \tag{S39}$$

$$= \left(-\frac{1}{s} \frac{L^*_{LT(s)} P}{h_a h_b E w} \right) \frac{\left(e^{\bar{x}} + e^{2\bar{L}} e^{-\bar{x}} \right)}{\left(1 - e^{2\bar{L}} \right)} \tag{S40}$$

$$= \left(-\frac{1}{s} \frac{L^*_{LT(s)} P}{h_a h_b E w} \right) \frac{\left(e^{\bar{x}} + e^{2\bar{L}-\bar{x}} \right)}{\left(1 - e^{2\bar{L}} \right)} \tag{S41}$$

$$= \left(\frac{1}{s} \frac{L^*_{LT(s)} P}{h_a h_b E w} \right) \frac{\left(e^{\bar{x}-\bar{L}} + e^{\bar{L}-\bar{x}} \right)}{\left(e^{\bar{L}} - e^{-\bar{L}} \right)} \tag{S42}$$

$$= \left(\frac{1}{s} \frac{L^*_{LT(s)} P}{h_a h_b E w} \right) \frac{\cosh\left(\bar{L} - \bar{x} \right)}{\sinh\left(\bar{L} \right)} \tag{S43}$$

$$\tag{S44}$$

to arrive at:

$$U_{(x)} = \frac{1}{s} \frac{P L^*_{LT(s)}}{h_a h_b E w} \frac{\cosh\left(\left(L - x \right) / L^*_{LT(s)} \right)}{\sinh\left(L / L^*_{LT(s)} \right)} \tag{S45}$$

Table S2 Time domain transform to the Laplace domain.

Time domain	Laplace domain
$\gamma(x,t)$	$U(x,s)$
$\frac{\partial \gamma}{\partial \bar{t}}$	$SU - \gamma_{(t=0)}$
$\frac{\partial^2 \gamma}{\partial \bar{x}^2}$	$\frac{\partial^2 U}{\partial \bar{x}^2}$
$\frac{\partial (\partial^2 \gamma)}{\partial \bar{t} \partial \bar{x}^2}$	$sL\{\frac{\partial^2 \gamma}{\partial \bar{x}^2}\} - \frac{\partial^2 \gamma}{\partial \bar{x}^2}\|_{(t=0)} = s\frac{\partial^2 U}{\partial \bar{x}^2} - \frac{\partial^2 \gamma}{\partial \bar{x}^2}_{(t=0)}$
$\frac{d\gamma}{dx}\|_{x=0} = \frac{P}{h_a h_b E}$	$\frac{dU}{dx}\|_{x=0} = \frac{1}{s}\frac{P}{h_a h_b E}$
$\frac{d\gamma}{dx}\|_{x=L} = 0$	$\frac{dU}{dx}\|_{x=L} = 0$

The constitutive expression for the Maxwell liquid is the following:

$$\frac{\partial \gamma}{\partial t} = \frac{1}{G_0} \frac{\partial \tau}{\partial t} + \frac{\tau}{\eta} \tag{S46}$$

Inserting (S5) into (S46) yields:

$$\frac{\partial \gamma}{\partial t} = \frac{h_a h_b E}{G_0}\frac{\partial(\partial^2\gamma)}{\partial t \partial x^2} + \frac{h_a h_b E}{\eta}\frac{\partial^2 \gamma}{\partial x^2} \tag{S47}$$

The Laplace transform on this, imposing the initial condition $\frac{\partial^2 \gamma}{\partial \bar{x}^2}_{(t=0)} = 0$, results in:

$$\frac{\partial^2 U}{\partial \bar{x}^2} = U\frac{s}{s h_a h_b E/G_0 + h_a h_b E/\eta} \tag{S48}$$

which similarly to Equation (S28) may be expressed in the form of Equation (S30) with an effective load transfer length unique to the Maxwell liquid:

$$L^*_{LT(s)} \equiv \left(\frac{S}{s h_a h_b E/G_0 + h_a h_b E/\eta}\right)^{-1/2} \tag{S49}$$

The standard linear solid constitutive expression is the following:

$$\gamma + \frac{\eta}{G_2}\frac{d\tau}{dt} = G_1\gamma + \frac{\eta(G_1+G_2)}{G_2}\frac{d\gamma}{dt} \tag{S50}$$

Plugging Equation (S5) into Equation (S50) yields:

$$h_a h_b E\frac{d\gamma^2}{dx^2} + h_a h_b E\frac{d}{dt}\left(\frac{d^2\gamma}{dx^2}\right) = G_1\gamma + \frac{\eta(G_1+G_2)}{G_2}\frac{d\gamma}{dt}$$

Which can be transformed into the Laplace domain:

$$h_a h_b E\frac{dU^2}{dx^2} + h_a h_b E s\left(\frac{d^2U}{dx^2}\right) = G_1 U + \frac{\eta\,(G_1+G_2)}{G_2} sU \tag{S51}$$

$$h_a h_b E\frac{dU^2}{dx^2}(1+s) = U\left(G_1 + \frac{\eta\,(G_1+G_2)}{G_2}s\right) \tag{S52}$$

$$\frac{dU^2}{dx^2} = U\left(\frac{\left(G_1 + \eta s\frac{G_1+G_2}{G_2}\right)}{h_a h_b E\,(1+s)}\right) \tag{S53}$$

Again, Equation (S53) may be expressed in the form of Equation (S30) with an effective load transfer length unique to the Standard linear Solid:

$$L^*_{LT(s)} \equiv \left(\frac{(G_1 + \eta s (G_1 + G_2)/G_2)}{h_a h_b E (1+s)} \right)^{-1/2} \tag{S54}$$

The Schapery approximation to transform from or to the Laplace domain is the following:

$$f(t) \approx sF(s)\big|_{s=\frac{1}{2t}} \tag{S55}$$

In our case, this is

$$\gamma_{(t)} \approx sU_{(s)}\big|_{s=\frac{1}{2t}} \tag{S56}$$

We can apply the Schapery inversion to Equation (S45) to arrive at:

$$\gamma = \frac{P L^*_{LT(t)}}{h_a h_b E w} \frac{\cosh((L-x)/L^*_{LT(t)})}{\sinh(L/L^*_{LT(t)})} \tag{S57}$$

Plugging Equation (S57) into Equations (S2) and (S3) yields the strain in the backing layer:

$$\varepsilon = -\frac{P}{h_b E w} \frac{\sinh((L-x)/L^*_{LT(t)})}{\sinh(L/L^*_{LT(t)})} \tag{S58}$$

Plugging Equation (S57) into Equation (S5) yields the adhesive stress:

$$\tau = \frac{P}{L^*_{LT(t)} w} \frac{\cosh((L-x)/L^*_{LT(t)})}{\sinh(L/L^*_{LT(t)})} \tag{S59}$$

Note that the effective load transfer length is now in the time domain ($L^*_{LT(s)} \rightarrow L^*_{LT(t)}$). The functional form for the effective load transfer length ($L^*_{LT(t)}$) for the Kelvin and Maxwell models is determined by completing the Schapery inversion, $s \rightarrow 1/2t$, on Equations (S29) and (S49) respectively (see Table (S3)). By inspection of Equation (S24), it is clear the functional form of the effective load transfer length in the linearly elastic case is exactly the conventionally defined load transfer length $L_{LT} = \sqrt{h_a h_b E/G}$.

Table S3 Time-dependent function that captures the evolution of the effective load transfer length for different constitutive models. Where $\bar{t} = t\eta/G$, with the shear modulus used in defining L_{LT} and $\bar{t}$ is G, G_0, and G_0, for the linearly elastic, Kelvin solid and Maxwell liquid cases respectively.

Model	Functional form of $L^*_{LT(t)}$	Normalized functional form $L^*_{LT(t)}$
linearly elastic	$L^*_{LT(t)} = L_{LT}$	$L^*_{LT(\bar{t})} = L_{LT}$
Kelvin-Voigt solid	$L^*_{LT(t)} = \left(\left(1+\frac{1}{2t}\frac{\eta}{G_0}\right)\frac{G_0}{h_a h_b E}\right)^{-1/2}$	$L^*_{LT(\bar{t})} = L_{LT}\cdot(\ 1+1/(2\bar{t}))^{-1/2}$
Maxwell liquid	$L^*_{LT(t)} = \sqrt{\left(\frac{h_a h_b E}{G_0}+2t\frac{h_a h_b E}{\eta}\right)}$	$L^*_{LT(\bar{t})} = L_{LT}\cdot\sqrt{(1+2\bar{t})}$
Standard linear Solid	$L^*_{LT(t)} = \sqrt{\frac{h_a h_b E(1+1/(2t))}{G_1+\eta\frac{(G_1+G_2)}{2G_2 t}}}$	

2.2 Comparison of Schapery Approximation to Numerical Solution

The adhesive shear strain for the Kelvin-Voigt model determined from the numerical solution to Equation (S27) and the approximate solution, directly from Equation (S57), are shown in figure S2 for $G_0 = 0.01$ MPa and $t_R = 30$ s. The agreement between the exact numerical solution and the approximate Schapery solution is good.

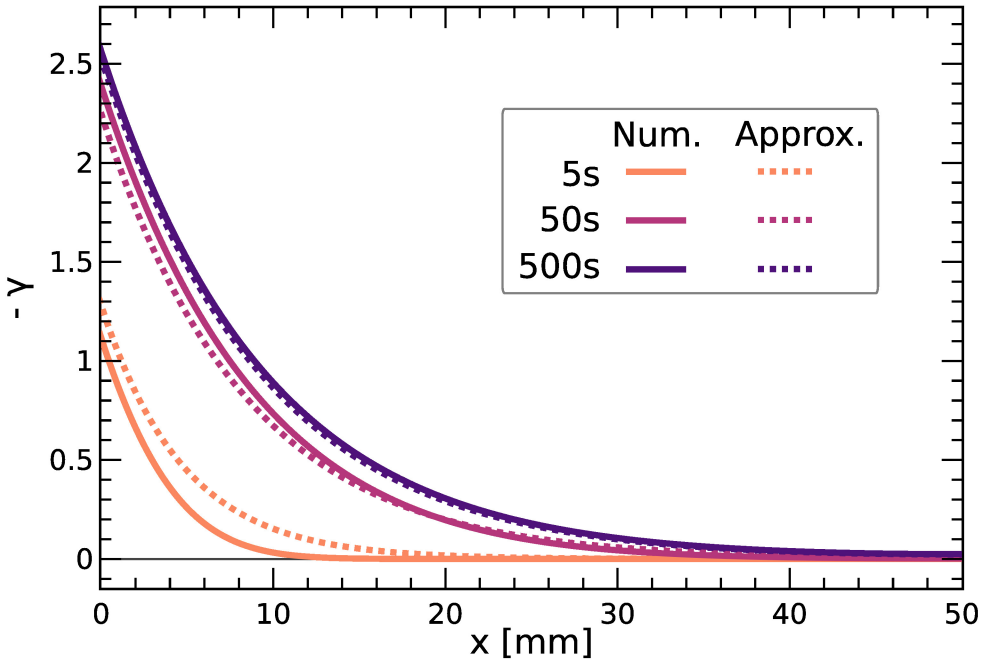

Fig. S2 Adhesive shear strain predicted by the Kelvin Shear Lag Model. Numerical solution and Approximate (Schapery inversion) solutions.

The adhesive shear stress for the Kelvin-Voight model from the numerical solution to Equation (S27) plugged into Equation (S5) for the adhesive shear stress τ, and the approximate solution, directly from Equation (S59), are shown in Figure S3. The agreement is good.

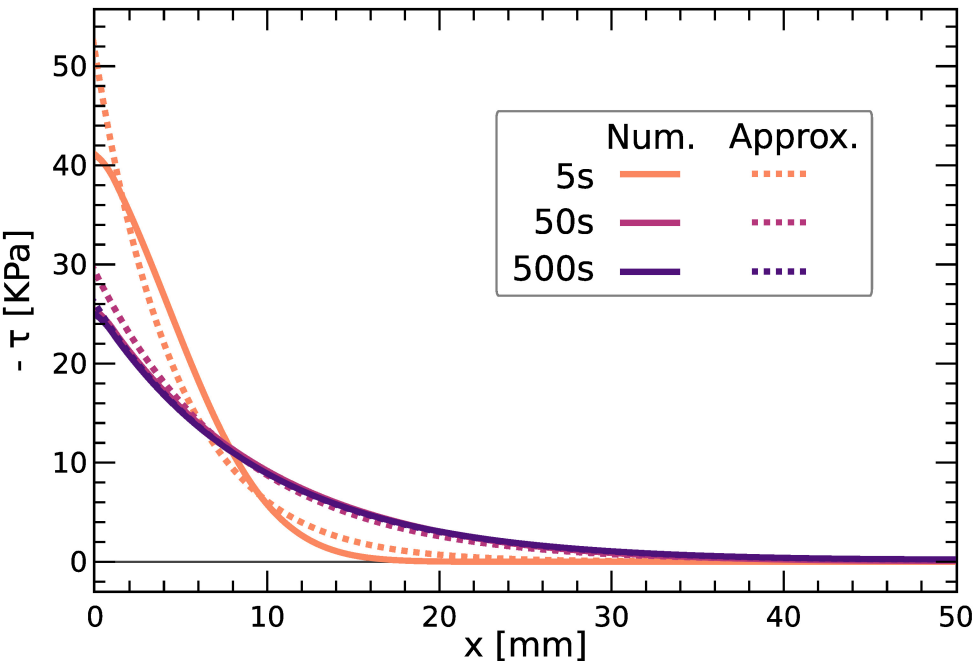

Fig. S3 Adhesive shear stress predicted by the Kelvin Shear Lag Model. Numerical solution and Approximate (Schapery inversion) solutions.

The adhesive shear strain for the Maxwell model from the numerical solution to Equation (S47) and the approximate solution from Equation (S57) are shown in Figure S4 for $G_o = 0.01$ MPa and $t_R = 3$ s. The agreement is good at short times and becomes increasing poor at long times.

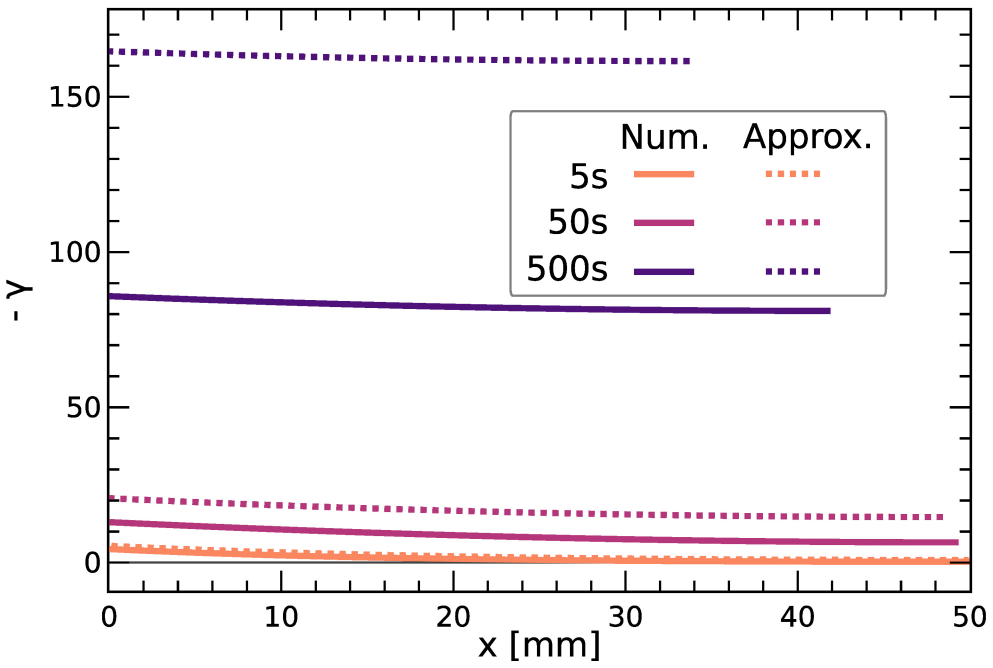

Fig. S4 Adhesive shear strain predicted by the Maxwell Shear Lag Model. Numerical solution and Approximate (Schapery inversion) solutions.

The adhesive shear stress for the Maxwell model from the numerical solution to Equation (S47) plugged into Equation (S5) for the adhesive shear stress τ, and the approximate solution, directly from Equation (S59), are shown in Figure S5. The agreement is good.

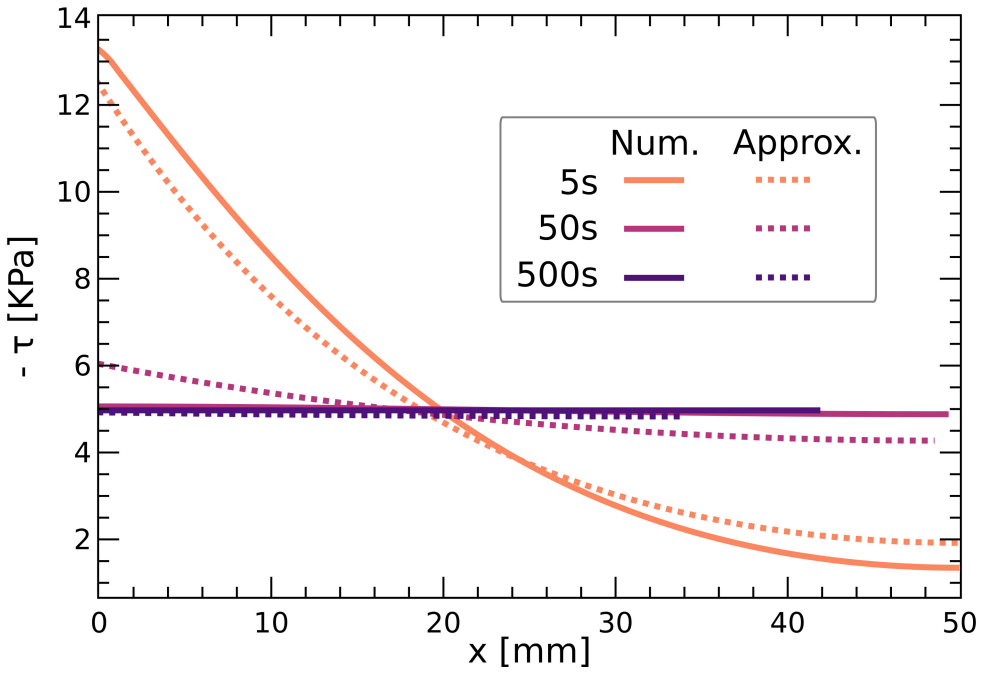

Fig. S5 Adhesive shear stress predicted by the Maxwell Shear Lag Model. Numerical solution and Approximate (Schapery inversion) solutions.

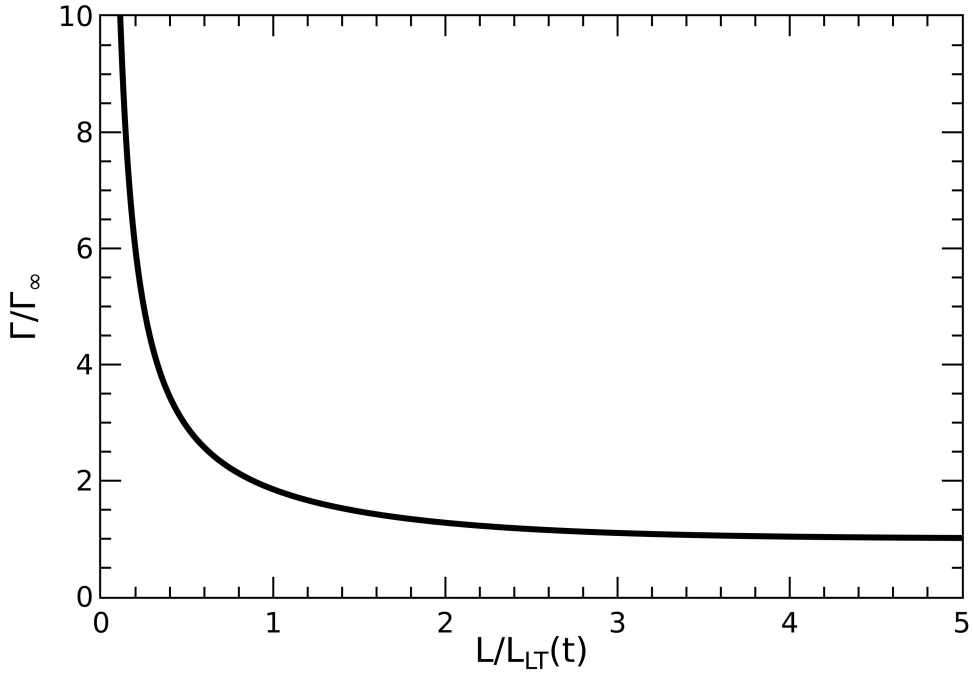

Fig. S6 The non-dimensionalized toughness of the bond as a function of bond length and time.

3 Lap Shear Experiment

The experimental setup is shown in Figure S7 A. The cameras, not shown in the picture, take images of the tape before and after the load is applied to apply a digital image correlation. An example of the digital image correlation positions tracked is shown in Figure S7 B.

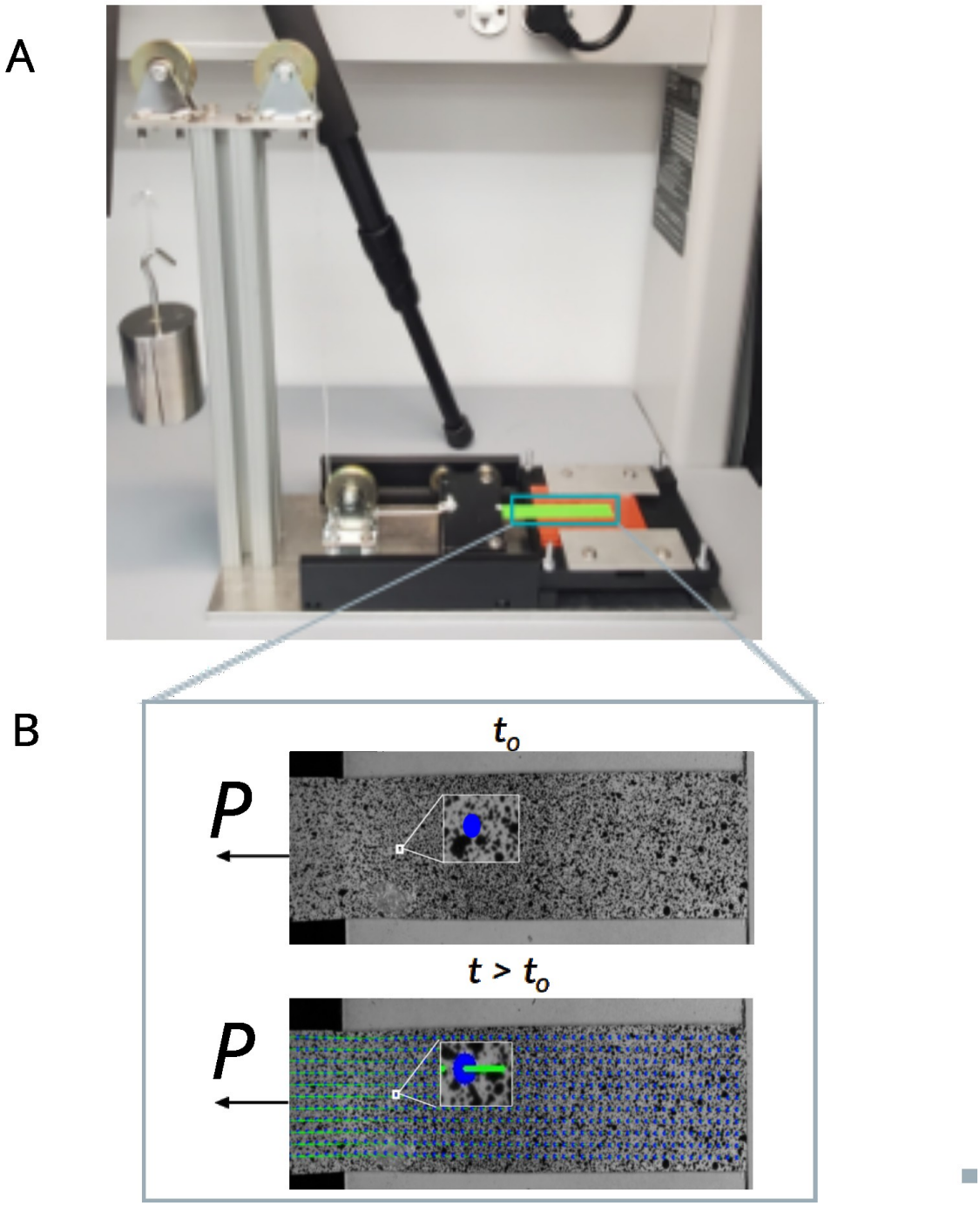

Fig. S7 (A) The zero degree lap shear experimental setup used. The weight is held connected through a series of pulley to a carriage which clamps the tape (shown in green for clarity). (B) Digital image correlation images taken during the experiment at t_0 before the load is applied and after, $t > t_0$, the load is applied.

The free region of tape consists of both PSA and the backing layer (see Figure S8). This region is primarily in tension and tension stresses would therefore be transferred directly from the free region of the PSA to the bonded region. The magnitude of the transferred axial stresses to the

bonded region contributed from the backing and the PSA layer can be approximated by their respective moduli.

Fig. S8 Scheme of the lap shear experiment illustrating the free region of PSA Figure (A). If the free region of PSA is neglected then Figure (B) is an accurate representation.

The LDPE backing layer has an elastic modulus of 170MPa and the time-dependent shear modulus of the PSA layer is *ca.* 0.1MPa at its highest. If the Poission's ratio of the PSA is assumed to be *ca.* 0.5, then the upper limit elastic modulus $E \approx 0.3MPa$. The tape in the free region can be modelled as the backing layer and PSA layer in parallel undergoing the same strain.

$$\varepsilon_{total} = \varepsilon_{PSA} = \varepsilon_{back}$$

$$\sigma_{PSA} = E_{PSA}\varepsilon_{PSA} = E_{PSA}\varepsilon_{total}$$
$$\sigma_{back} = E_{back}\varepsilon_{back} = E_{back}\varepsilon_{total}$$

$$E_{back} = 170MPa$$
$$E_{PSA} \approx 0.3MPa$$
$$\frac{\sigma_{PSA}}{\sigma_{backing}} = \frac{E_{PSA}\varepsilon_{total}}{E_{back}\varepsilon_{total}} = \frac{E_{PSA}}{E_{backing}} \approx 0.002$$

Therefore, a majority of axial stresses in the free region are held by the backing layer and the contributions of the axial stresses from the free region of PSA to the bonded region of PSA are negligible - Figure S8 (B) is an appropriate model for the experiment. That is, the PSA exhibits primarily shear stresses from the backing layer and the force balance of the shear lag model is applicable.

The elastic modulus of the LDPE backing layer which the PSAs were cast onto was determined by a tensile test using an Instron 34TM5. Two strain rates were tested - 1%/minute and 10%/minute - and are shown in Figure S9. The elastic modulus was determined by averaging the stress, at 1% strain, between the two strain rates. This results in an elastic modulus of 170 MPa.

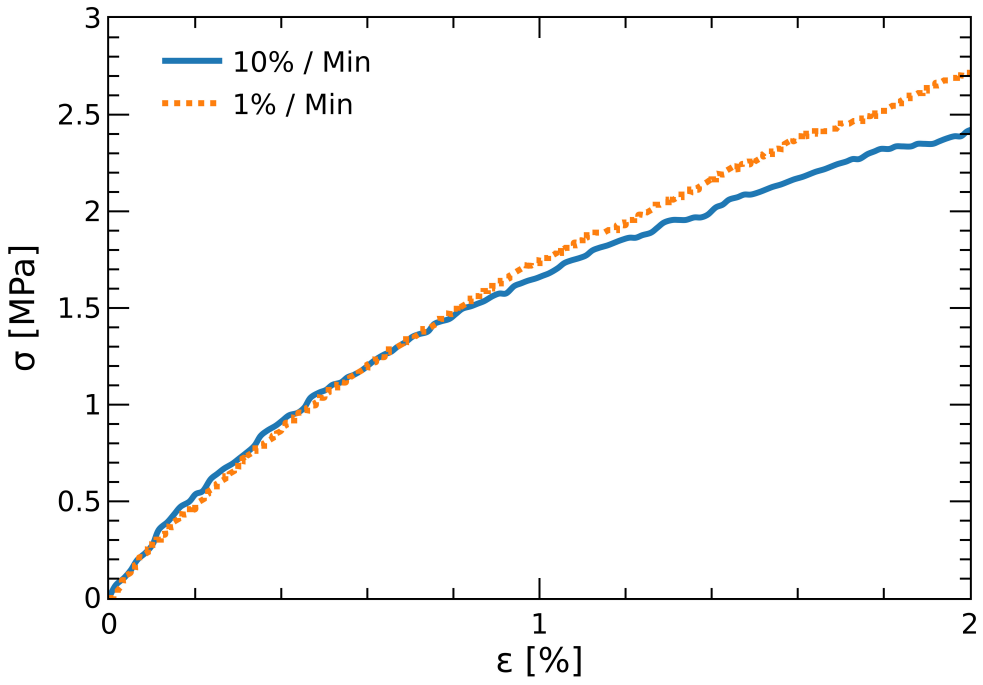

Fig. S9 Tensile test of the LDPE backing layer.

3.1 Experimental Strain and Stress

3.1.1 Direct Calculation of Shear Stress

The experimental shear stress in the adhesive layer was determined from rational function fits to the backing strain. Figures S10 and S11 illustrate these fits for a bond length of 50mm and demonstrate a very good fit to the strain. The apparent sinusodial deviations from the fits in Figure S10 are likely artifacts of the digital image correlation analysis, as there is no other conceivable explanation for these fluctuations.

The fits to the backing strain for the uncrosslinked PSA lap shear tests are shown below and plotted in Figure S10:

$$\varepsilon_{5\text{ s}} = \frac{-0.006697x + 0.3302}{x + 20.9} \tag{S60}$$

$$\varepsilon_{50\text{ s}} = \frac{-0.04932x + 2.407}{x + 125.4} \tag{S61}$$

$$\varepsilon_{500\text{ s}} = -0.0004854x + 0.01874 \tag{S62}$$

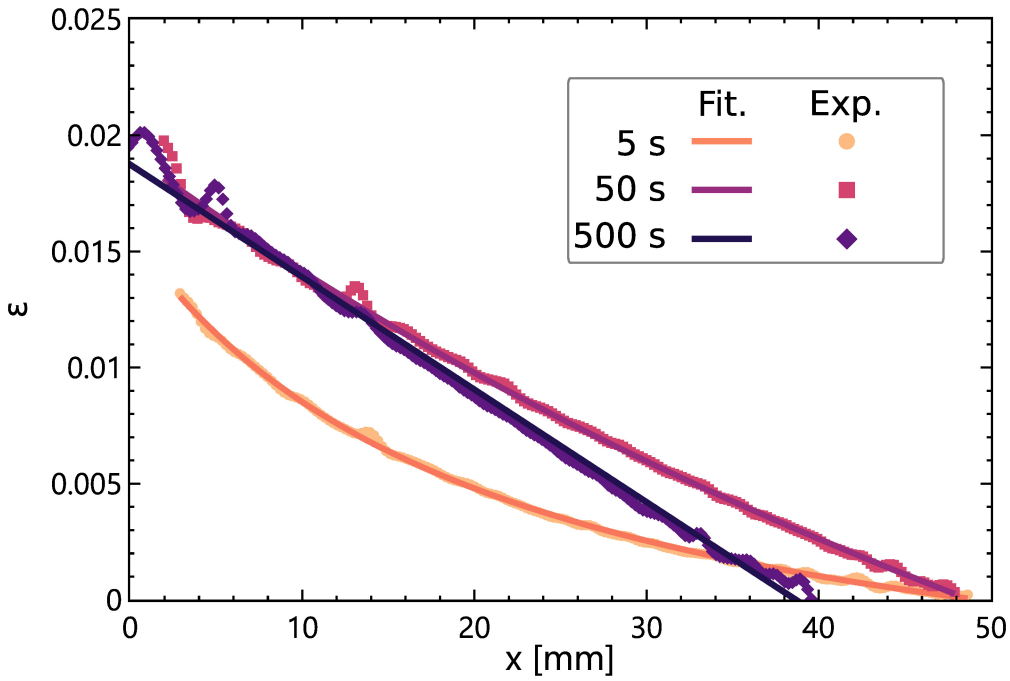

Fig. S10 The strain in the backing layer for the uncrosslinked PSA, experimental results and fits.

The fits to the backing strain for the 1% crosslinked PSA lap shear tests are shown below and plotted in Figure S10:

$$\varepsilon_{5\text{ s}} = \frac{-0.0005839x^2 + 0.01107x + 0.7332}{x^2 + 6.248x + 60.58} \tag{S63}$$

$$\varepsilon_{50\text{ s}} = \frac{-0.0008086x^2 + 0.005234x + 1.595}{x^2 + 11.09x + 92.27} \tag{S64}$$

$$\varepsilon_{500\text{ s}} = \frac{-0.0009708x^2 - 0.001085x + 2.432}{x^2 + 12.27x + 118.7} \tag{S65}$$

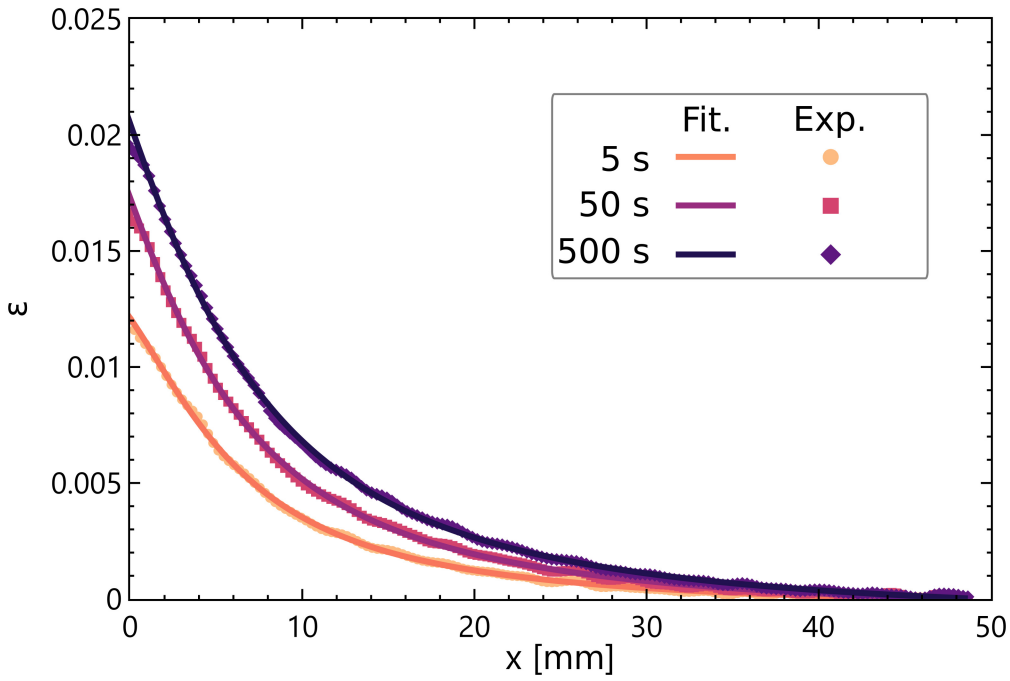

Fig. S11 The strain in the backing layer for the 1% crosslinked PSA, experimental results and fits.

The shear strain, for the uncrosslinked (0%) and 1wt % crosslinked polymers, computed directly from Digital Image Correlation are shown in Figure S12 (row 1). The backing strain, from the derivative of displacements, is shown in row 2. The adhesive shear stress determined from an analytical derivative of the backing strain equations inserted into Equation S5 are shown in row 3. It is worth noting that rather if a numerical derivative of the backing strain were taken to determine the adhesive stress, the noise in the adhesive stress would be unacceptably large and the large amount of smoothing required for it to be meaningful would significantly reduce data integrity.

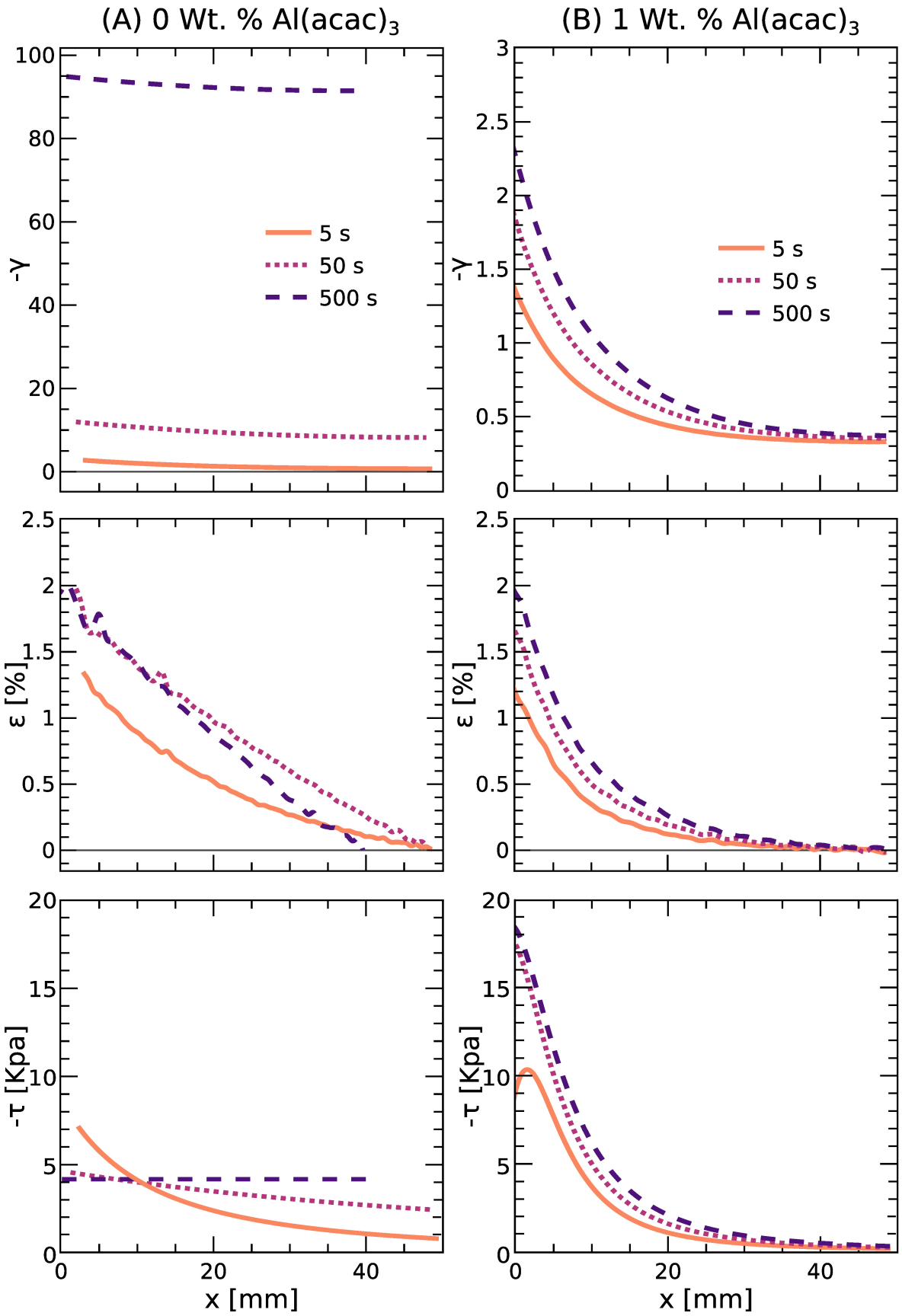

Fig. S12 Digital Image Correlation measured shear strain of the adhesive layer, axial strain in the backing layer, and shear stress in the adhesive layer.

3.1.2 Experimental Fits to Approximate Solution of Shear Lag Model

The backing strains were fit to equation (S58) to estimate the effective load transfer length over time by allowing the effective load transfer length ($L^*_{LT(t)}$) to be a fitting parameter. Note that the backing layer did not exhibit the expected strain of 0.28. This may be attributed some combination of, resistance of the load train, creep of the backing layer, or the adhesive layer in the free region. Still a reasonable fit may be found if the load (P) is offset by a constant such that the fit of the strain reaches the actual strain of 0.2, (i.e. assuming the applied load is 70% of that actually applied). The fits are shown for the 50mm bond length tapes of 0 wt % and 1wt % crosslinked in figures S13 and S14 respectively.

The effective load transfer ($L^*_{LT(t)}$) from the fits to equation are shown over time in figure S15. Note that $L^*_{LT(t)}$ approaches the bond length for the 0 wt % and does increase further. This is likely due to fitting the backing strain rather than the adhesive strain, thus ignoring the bulk deformation, and is therefore an underestimate of $L^*_{LT(t)}$. Also, note that $L^*_{LT(t)}$ decreases dramatically just prior to the bond failing, this is due to the overlap length changing and as the tape moves. In this regime the mechanics should include delamination, slippage and damage, to capture the true stress distribution and is therefore outside the scope of this model. The 1wt % crosslinked PSA exhibits a much smaller ($L^*_{LT(t)}$) that grows at a much slower rate.

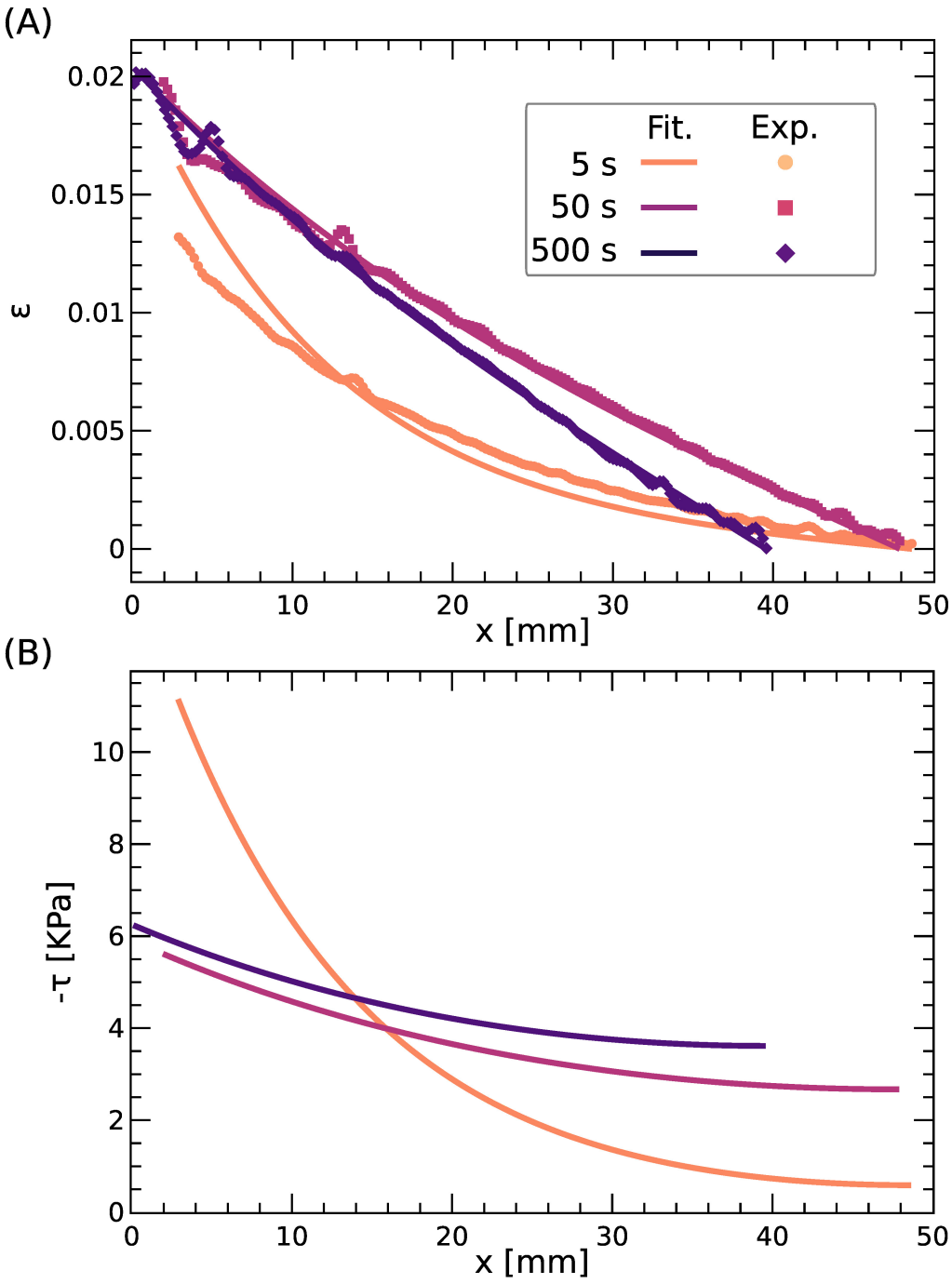

Fig. S13 Strain and Stress distributions for the uncrosslinked PSA on a tape of 50mm long. (A) Experimentally measured strain and fits to the Schapery approximate solution of the shear lag model (equation (S58)) by fitting the effective load transfer length. (B) Adhesive Shear Stress computed by equation (S59) using the fitted effective load transfer length.

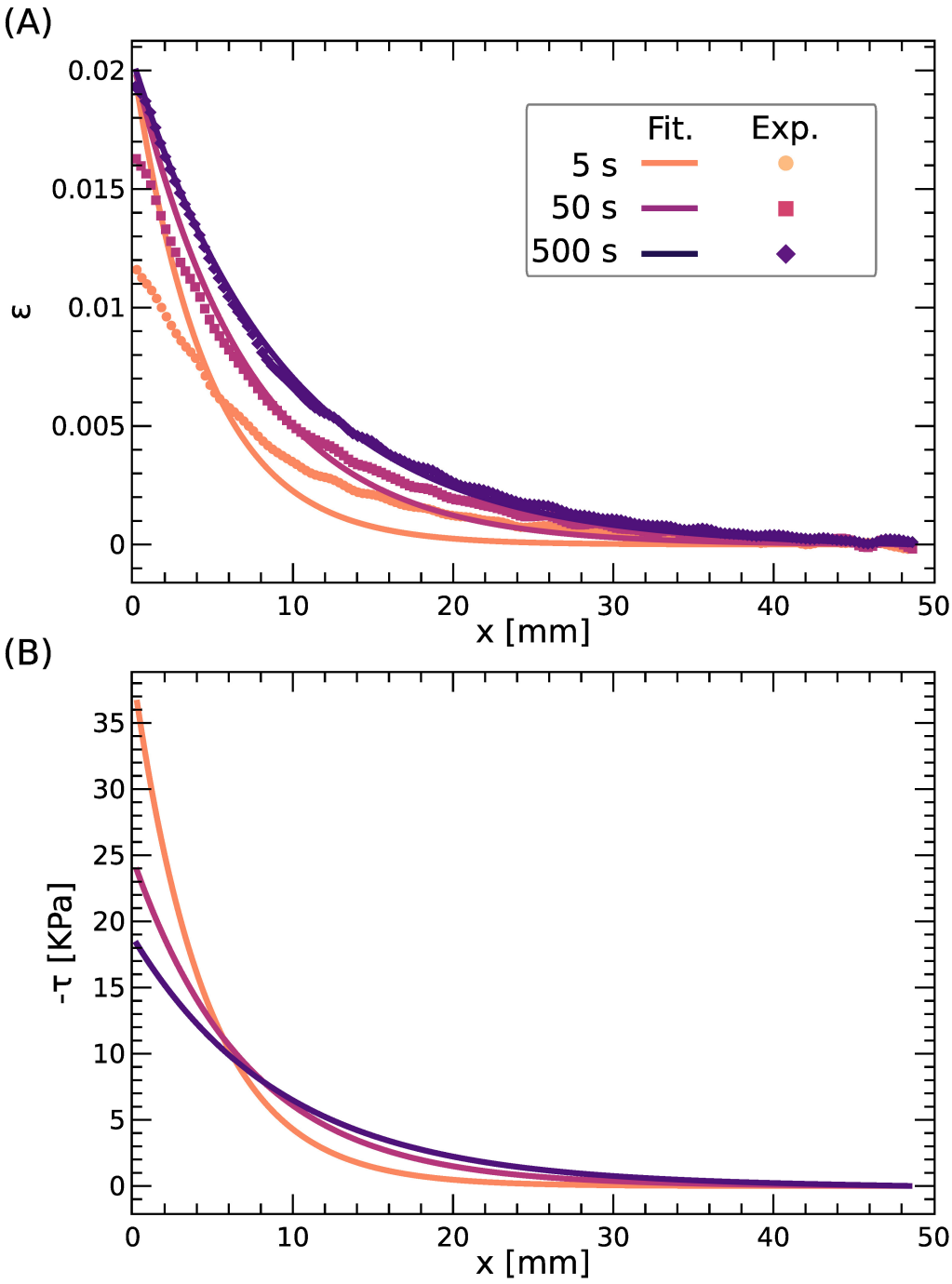

Fig. S14 Strain and stress distributions for the 1wt % PSA on a tape of 50mm long. (A) Experimentally measured strain and fits to the Schapery approximate solution of the shear lag model (equation (S58)) by fitting the effective load transfer length. (B) Adhesive Shear Stress computed by equation (S59) using the fitted effective load transfer length.

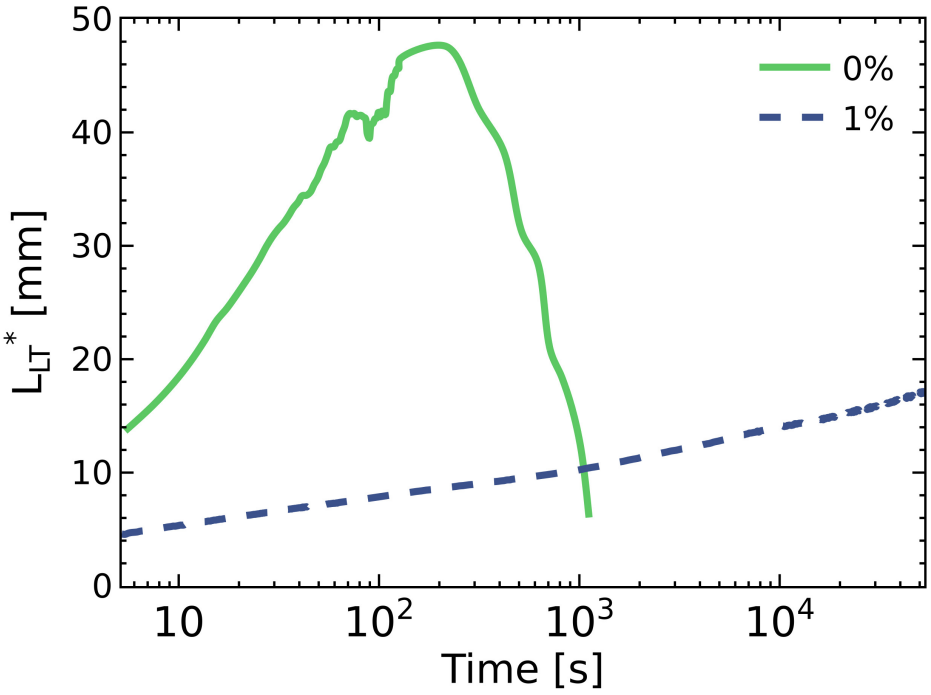

Fig. S15 Effective load transfer length ($L^*_{LT}(t)$) determined by fitting equation (S58) to the backing strain of the 50mm bond lengths for the 0 wt % and 1wt % crosslinked PSAs.

3.2 Material Properties of the Polymers

The molecular weight distribution of the poly(2-ethylhexyl acrylate-co-acrylic acid) copolymer measured by Gel Permeation Chromatography (GPC), eluting with tetrahydrafuran over a T6000M column (Malvern Panalytical) is shown in Figure S16.

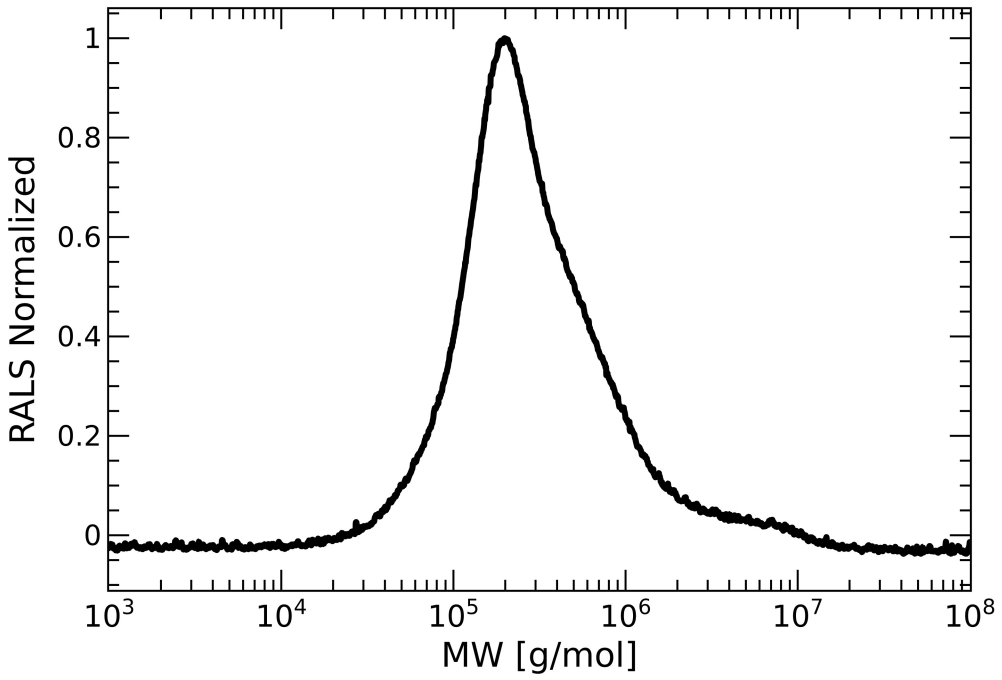

Fig. S16 Gel Permeation Chromatography of the family of polymers.

The last of the three temperature sweeps of the family of crosslinked polymers from Differential Scanning Calorimetry (DSC 250 TA Instruments Inc.) at 1 ^{o}C/min., are shown in Figure S17.

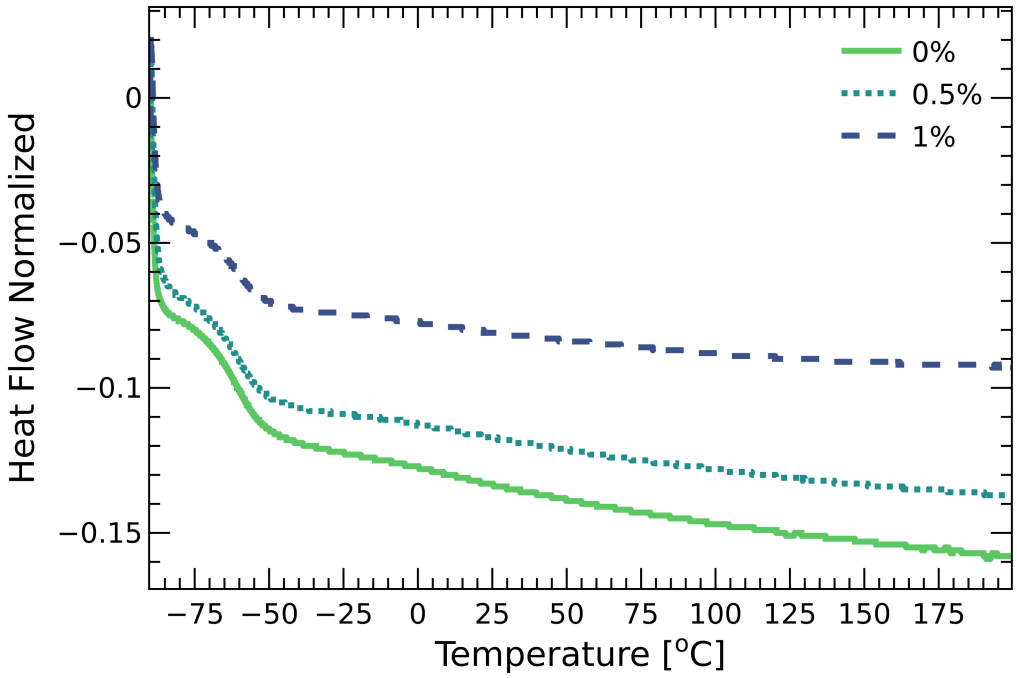

Fig. S17 Digital Scanning Calorimetry of the family of polymers after crosslinking.

3.3 Displacements at the Trailing Edge

The velocity of the tape measured during the lap shear experiment was computed by the numerical time derivative of the displacements as measured by Digital Image Correlation (DIC) at the trailing edge of the tape. A moving average of ten (10) consecutive displacements in time was computed and with this, central differences was applied to the averages to compute the velocity (see dotted lines in Figure S18). This procedure reduced the noise amplification associated with the central differences. Some artifacts of the DIC are still present, likely due to lighting fluctuations during the experiment, as seen at *ca.* 10 seconds and *ca.* 10,000 seconds for the 1% crosslinked sample in Figure S18. Fits to the velocity using the empirical equation $\frac{\partial \delta_L}{\partial t} = \alpha t^{\beta}$, within the time ranges (5 s, 30 s), (5 s, 1000 s) and (5 s, 4000 s) for the 0%, 0.5% and 1% samples respectively, are shown as solid lines in Figure S18.

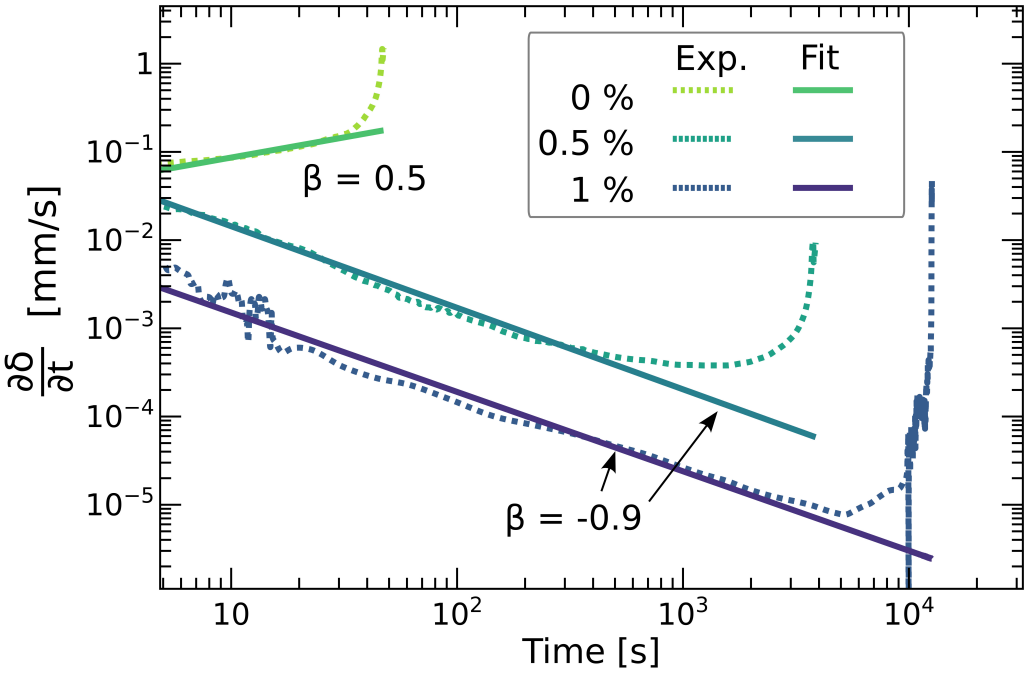

Fig. S18 Displacement rate as computed by the derivative of the displacement (dotted lines) and fits to the displacement using the empirical equation $\frac{\partial\delta}{\partial t} = \alpha t^{\beta}$ (solid lines).

The critical displacement was determined by fitting a linear curve to the displacement in the regime after the initial displacement and the prior to the final failure. The extrapolation of this linear fit to the time of failure provides the critical displacement and time (δ_c and t_c) as seen in the intercept of the dotted lines in Figure S19.

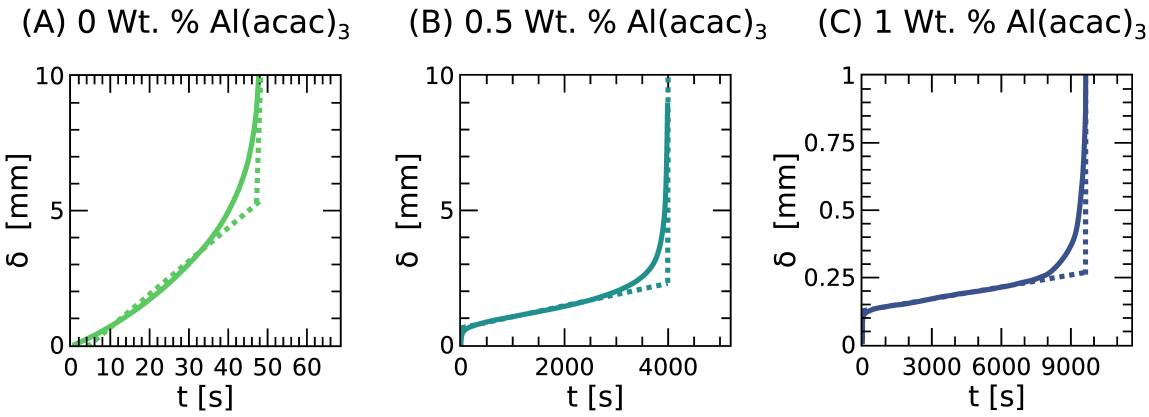

Fig. S19 Displacement of the trailing edge of the tapes for 10mm bond lengths. Linear fits of the displacement are shown as dotted lines. Vertical lines intersect from the last data-point measured and the extrapolated linear fit. This intersection represents the critical displacement and time.

References

1 C.-Y. Hui, Z. Liu, H. Minsky, C. Creton and M. Ciccotti, *Soft Matter*, 2018, **14**, 9681–9692.

2 Z. Liu, H. Minsky, C. Creton, M. Ciccotti and C.-Y. Hui, *Extreme Mechanics Letters*, 2019, **32**, 100518.